# Lightweight Electrochemical Hybrid Modeling Approach for Li-ion Batteries using Gaussian Process Regression

Jackson Fogelquist and Xinfan Lin

Abstract—The development of next-generation battery management systems needs models with enhanced performance to enable advanced control, diagnostic, and prognostic techniques for improving the safety and performance of lithium-ion battery systems. Specifically, battery models must deliver efficient and accurate predictions of physical internal states and output voltage, despite the inevitable presence of various system uncertainties. To facilitate this, we propose a lightweight hybrid modeling framework that couples a high-fidelity physics-based electrochemical battery model with a computationally-efficient Gaussian process regression (GPR) machine learning model to predict and compensate for errors in the electrochemical model output. This is the first time that GPR has been implemented to predict the output residual of an electrochemical battery model, which is significant for the following reasons. First, we demonstrate that GPR is capable of considerably improving output prediction accuracy, as evidenced by an observed average rootmean-square prediction error of 7.3 mV across six testing profiles, versus  $119 \, mV$  for the standalone electrochemical model. Second, we employ a data sampling procedure to exhibit how GPR can use sparse training data to deliver accurate predictions at minimal computational expense. Our framework yielded a ratio of computation time to modeled time of 0.003, indicating ample suitability for online applications.

## I. INTRODUCTION

The widespread adoption of lithium-ion (Li-ion) batteries has spurred significant efforts toward developing the next generation of battery management systems (BMSs), often termed advanced BMSs, which seek to enhance battery safety and performance through features such as online health monitoring [1], [2], optimal charging control [3], [4], and remaining useful life prognostics [5]. These features require a battery model that is capable of delivering accurate voltage output predictions (i.e., for use in feedback control and estimation) while maintaining the fidelity and physical significance of the internal states and parameters (i.e., for optimal control and degradation monitoring). Accordingly, physics-based electrochemical battery modeling is an active research domain, in which first-principles models are being implemented in BMS applications to encode the physical mechanisms of battery operation [6]. On the other hand, researchers are avidly investigating the use of machine learning (ML) methods for predicting battery performance, which base predictions on statistically extracted relationships from data [7]. Finally, hybrid modeling is an emerging approach that combines the complementary strengths of the physicsbased and ML modeling paradigms [8], [9].

Jackson Fogelquist and Xinfan Lin are with the Department of Mechanical and Aerospace Engineering, University of California, Davis, CA 95616, USA, corresponding author e-mail: lxflin@ucdavis.edu

Physics-based electrochemical models are derived from first principles and thus maintain the physical significance of the states and parameters through explicit consideration of the underlying electrochemical processes. The prevailing electrochemical model is the Doyle-Fuller-Newman (DFN) model [10], from which numerous control-oriented reducedorder models have been developed to improve computational efficiency while maintaining fidelity, e.g., the single particle model [11]. These models enable high prediction accuracy, efficient health diagnosis (i.e., through the monitoring of trends in health-related parameters), and safer and betterperforming model-based control (i.e., through the availability of physical internal states) [6], [12]. However, electrochemical models comprise systems of partial differential equations (PDEs) with dozens of parameters, making them computationally demanding and difficult to identify. Furthermore, even a correctly identified model with physically-accurate parameters will yield output prediction errors due to unmodeled system dynamics and other uncertainties [13].

ML models are capable of identifying and exploiting high-dimensional patterns in system data, enabling accurate predictions without considering the underlying physical processes [8]. Accordingly, these models are favorable for systems in which the physical processes are not sufficiently understood, such that a suitable physics-based model cannot be developed [9]. ML models are commonly applied in Liion battery applications for predicting state of charge (SOC), state of health (SOH), and remaining useful life (RUL), using algorithms such as artificial neural networks, support vector machines, relevance vector machines, and Gaussian process regression (GPR) [7], [14]. While these methods have been demonstrated to yield excellent prediction accuracy, they are subject to several fundamental limitations, including limited model interpretability, large training data requirements, and poor generalizability outside of the conditions spanned by the training data [8], [9].

Hybrid models combine physics-based and ML methods to leverage the respective strengths of each, i.e., to retain the physical significance and generalizability of the model while compensating for unmodeled physics through relationships extracted from data [15]. An important hybrid modeling topology is the residual model, which uses ML to predict the error between the output measurement and the physics-based model prediction, i.e., the battery voltage residual. The residual is then added to the physics-based model output prediction to compensate for the various model/measurement uncertainties, e.g., unmodeled dynamics, sensor bias/noise, and discretization errors, among others. In [16], a recurrent

neural network was trained to predict the voltage residual between the full-order DFN model and a reduced-order single particle model, based on the input current and residual feedback. Later, [17] employed both polynomial regression and GPR to predict the voltage residual between experimental measurements and the output of an equivalent circuit model. In [18], a feedforward neural network was implemented to predict the voltage residual between the DFN model and single particle model, and later between experimental data and the output of an equivalent circuit model. Most recently, [15] compared the performance of a feedforward neural network, regression tree, and random forest algorithm for predicting the voltage residual between experimental measurements and the output of an enhanced single particle model. These works are encouraging in that they demonstrate the capability for hybrid models to compensate for the model/measurement uncertainties inherent to the physicsbased modeling paradigm, yet they are limited in that they contain large, computationally-demanding ML models with substantial training data requirements.

The objective of this work is to develop a lightweight GPR-based hybrid residual model that delivers accurate output voltage predictions while facilitating the accurate estimation of the physics-based electrochemical parameters under uncertainty. The use of GPR for voltage residual modeling has been scarcely explored in the battery literature, and to our knowledge, this is the first time GPR has been coupled with an electrochemical model for this task. This is an important contribution for the following reasons. First, our implementation of GPR bears several benefits over the conventional use of neural networks for residual modeling. Specifically, the training procedure is fundamentally more efficient, as the number of trainable parameters is typically one to two orders of magnitude less than that of neural networks [19]. enabling substantially faster computations [14]. In addition, GPR automatically ingrains the confidence interval in the prediction result, performs well under sparse training data, and is highly interpretable due to the simple probabilistic structure [7], [19]. Second, existing hybrid residual models focus solely on improving voltage prediction accuracy without considering the accuracy and physical significance of the physics-based model parameters. By representing the model/measurement uncertainty (i.e., voltage residual) as a Gaussian process, it is possible to consider the influence of uncertainty in parameter estimation through the maximum likelihood estimation approach [20], which could facilitate the parameterization of the hybrid model. This is significant because a correctly parameterized physics-based model is critical for degradation monitoring (through tracking trends in health-related parameters), accurately estimating physical states (through the dependence of estimation algorithms on the physical model/parameters), and improving controller performance (through reliable knowledge of the physical states). The proposed framework opens the door to exploring this capability, which we leave for future work. In this work, we focus on efficiently achieving high output prediction accuracy.

#### II. ELECTROCHEMICAL LI-ION BATTERY MODEL

This section briefly summarizes the Li-ion battery electrochemical model, namely, the widely-adopted single particle model with electrolyte dynamics (SPMe) [21], [22], which will serve as the foundation for the hybrid model developed in Section IV. The SPMe predicts the battery internal physical states and output terminal voltage (V) from the input current (I). It is derived from the full-order DFN model under the simplification that reaction current density (and thus solid-phase ionic concentration) is uniform across each electrode. Accordingly, the electrochemical mechanisms in each electrode (i.e., lithium diffusion and (de)intercalation) are captured with a single particle, and both electrode particles interface with the electrolyte diffusion dynamics across the anode, separator, and cathode.

The output terminal voltage is expressed as

$$V = U_p(c_{se,p}) - U_n(c_{se,n}) + \phi_{e,p}(c_{e,p}) - \phi_{e,n}(c_{e,n}) + \eta_p(c_{se,p}, c_{e,p}) - \eta_n(c_{se,n}, c_{e,n}) - IR_l,$$
(1)

which relies upon the differences between the cathode and anode potentials, denoted by subscripts p and n, respectively. The open-circuit potentials (OCPs) U represent the equilibrium potential of each electrode as a nonlinear function of the electrode particle surface lithium concentration  $c_{se}$ . The evolution of  $c_{se}$  is governed by the solid-phase ionic diffusion dynamics according to Fick's second law. The electrolyte potentials  $\phi_e$  are driven by the ionic concentration gradient across the electrolyte, which is characterized by the electrolyte lithium concentration at each electrode boundary  $c_{e,i}$ . The evolution of  $c_e$  is governed by the ionic diffusion dynamics in the electrolyte according to Fick's second law. The overpotentials  $\eta$  drive the (de)intercalation reaction current densities according to the Butler-Volmer equation. The lumped resistance term  $R_l$  captures the voltage drop across the various Ohmic resistances (i.e., of the electrolyte, current collectors, and solid-electrolyte interphase layer).

Finally, it is important to define the SOC, which indicates the fraction of available charge in the cell. It is typically based on the electrode surface concentration  $c_{se}$  in terms of the stoichiometry numbers, where  $\theta_{surf} = \frac{c_{se}}{c_s^{max}}$  is the surface stoichiometry number and  $c_s^{max}$  denotes the maximum solid-phase concentration. The stoichiometry limits at the fully charged and discharged conditions are denoted as  $\theta_1$  and  $\theta_0$ , respectively. The surface SOC is averaged across the two electrodes as

$$SOC_{surf} = \frac{1}{2} \left( \frac{\theta_{surf,p} - \theta_{0,p}}{\theta_{1,p} - \theta_{0,p}} + \frac{\theta_{surf,n} - \theta_{0,n}}{\theta_{1,n} - \theta_{0,n}} \right).$$
 (2)

Alternatively, the bulk SOC can be defined by the electrode bulk concentration  $\overline{c}_s$ , which represents the total molar concentration of lithium in the electrode particle. The bulk SOC is thus dependent on the bulk stoichiometry number  $\theta_{bulk} = \frac{\overline{c}_s}{\overline{c}^{max}}$ , as

$$SOC_{bulk} = \frac{1}{2} \left( \frac{\theta_{bulk,p} - \theta_{0,p}}{\theta_{1,p} - \theta_{0,p}} + \frac{\theta_{bulk,n} - \theta_{0,n}}{\theta_{1,n} - \theta_{0,n}} \right).$$
(3)

The bulk SOC differs from the surface SOC in that it does not incorporate the diffusion dynamics across each particle, but rather is a perfect integrator of the reaction current density to account for the accumulation of lithium ions in the particles. The reader is referred to [22] for the full details of the model.

### III. GAUSSIAN PROCESS REGRESSION

The purpose of this section is to provide a brief overview of GPR, which will be implemented to predict the voltage residual for the hybrid model in Section IV. The objective of GPR (and other regression methods) is to characterize an unknown continuous relationship between observed system inputs  $\boldsymbol{X} = [\boldsymbol{x}_1, \dots, \boldsymbol{x}_N]$  and outputs  $\boldsymbol{y} = [y_1, \dots, y_N]$ , where the inputs may be multidimensional such that  $\boldsymbol{x}_i = [x_{i,1}, \dots, x_{i,d}]^T$ . Here, N denotes the number of observations and d specifies the number of input signals per observation.

GPR operates under the fundamental assumption that the unknown input-output relationship can be represented as a Gaussian process, i.e., a collection of jointly Gaussian random variables f(x) defined by a mean function m(x) and covariance function k(x, x') [19],

$$f(\mathbf{x}) \sim \mathcal{GP}(m(\mathbf{x}), k(\mathbf{x}, \mathbf{x}')),$$
 (4)

where

$$m(\mathbf{x}) = \mathbb{E}[f(\mathbf{x})],\tag{5}$$

$$k(\boldsymbol{x}, \boldsymbol{x}') = \mathbb{E}\left[ \left( f(\boldsymbol{x}) - m(\boldsymbol{x}) \right) \left( f(\boldsymbol{x}') - m(\boldsymbol{x}') \right) \right]. \tag{6}$$

For our application of predicting the voltage residual, which has an ideal value of zero, we let the mean function be m(x) = 0. Thus, the Gaussian process is defined entirely by the covariance function, which encodes the fundamental behavior of the prediction model. We have selected the squared exponential covariance function due to its widespread adoption and versatility in the literature [19], [23],

$$k(\boldsymbol{x}, \boldsymbol{x}') = \sigma_f^2 \exp\left(-\frac{1}{2}(\boldsymbol{x} - \boldsymbol{x}')^T \boldsymbol{L}(\boldsymbol{x} - \boldsymbol{x}')\right),$$
 (7)

which is characterized by the hyperparameters  $\sigma_f^2$  and  $L=\mathrm{diag}(l)^{-2}$ , where  $l=[l_1,\ldots,l_d]$  comprises the length-scale for each input signal. Conceptually, the squared exponential function specifies the extent to which two input vectors x and x' are correlated, based on their proximity to one another. The covariance matrices associated with the input training data X and a given set of input test points  $X_*$  can be formed through elementwise evaluation of Eqn. (7) under the respective input data sets, i.e., K=K(X,X),  $K_*=K(X,X_*)$ , and  $K_{**}=K(X_*,X_*)$ . Finally, we have incorporated i.i.d. Gaussian observation noise with variance  $\sigma_n^2$ , such that the noisy training data covariance matrix is defined as  $K_n=K+\sigma_n^2I$  [19].

Letting  $f_*$  denote the function predictions under the input test points  $X_*$ , the joint distribution of the observed outputs y and function predictions  $f_*$  can be conditioned on the observations (X, y) to yield the joint posterior distribution [19],

$$f_*|X, y, X_* \sim \mathcal{N}\left(\overline{f}_*, cov(f_*)\right),$$
 (8)

with

$$\overline{\boldsymbol{f}}_* = \boldsymbol{K}_*^T \boldsymbol{K}_n^{-1} \boldsymbol{y}, \tag{9}$$

$$cov(f_*) = K_{**} - K_*^T K_n^{-1} K_* + \sigma_n^2 I.$$
 (10)

Thus, for a given set of input test points  $X_*$ , the outputs can be predicted as the conditional mean  $\overline{f}_*$  with a confidence interval specified by the conditional variance diag  $(cov(f_*))$ . This is a major advantage of GPR over other ML techniques, as the confidence interval can critically inform how predictions should be used in practice [24].

The hyperparameters for the squared exponential covariance function in Eqn. (7) are  $\theta = [\sigma_n^2, \sigma_f^2, l_1, \dots, l_d]$ , which can be efficiently tuned by maximizing the log marginal likelihood of the prediction [19], [24],

$$\max_{\boldsymbol{\theta}} \log p(\boldsymbol{y}|\boldsymbol{X}, \boldsymbol{\theta}) = -\frac{1}{2} \boldsymbol{y}^{T} \boldsymbol{K}_{n}^{-1} \boldsymbol{y} - \frac{1}{2} \log |\boldsymbol{K}_{n}| - \frac{N}{2} \log 2\pi.$$
(11)

Maximizing the log marginal likelihood has been shown to automatically mitigate overfitting through the ingrained trade-off between data fit and model complexity [19]. However, the number of computer operations required to invert  $K_n$  scales cubically with the number of training data points, which limits a tractable training data set to several thousand points for modern workstations [23]. We address this through a data sampling procedure presented in the subsequent section.

#### IV. HYBRID MODEL FORMULATION

The SPMe electrochemical battery model was combined with the GPR residual model to form the proposed hybrid model, illustrated in Fig. 1. At a given time k, the SPMe receives the input current I and returns the predicted output voltage  $V_{SPMe}$  and internal states. The GPR model receives the same input current and a subset of predicted internal states from the SPMe, s. It returns a prediction of the residual  $\delta V$ , which is summed with the SPMe voltage prediction to yield the final output voltage V.

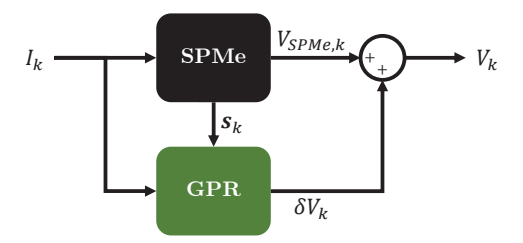


Fig. 1. Schematic of proposed hybrid model.

Three of the SPMe internal states were applied as inputs to the GPR model, namely, the surface SOC, bulk SOC, and anode electrolyte concentration, i.e.,  $s_k = [SOC_{surf,k}, SOC_{bulk,k}, c_{e,n,k}]^T$ . These states were selected to succinctly encode the information contained in the six SPMe concentration states. Specifically, the surface SOC was selected because it conveniently captures the battery dynamic behavior, e.g., diffusion, contained in the surface

TABLE I
SUMMARY OF INPUT CURRENT PROFILES

| Group      | Input Profile Ty   |             | Initial | Data   |
|------------|--------------------|-------------|---------|--------|
|            |                    | Type        | SOC (-) | Points |
| Training   | 1C Discharge       | Constant    | 1       | 11,110 |
|            | 2C Discharge       | Constant    | 1       | 5,353  |
|            | 3C Discharge       | Constant    | 1       | 3,471  |
|            | 4C Discharge       | Constant    | 1       | 2,514  |
|            | 5C Discharge       | Constant    | 1       | 1,929  |
|            | 1C FUDS            | Drive Cycle | 0.5     | 6,000  |
| Validation | 2.5C Discharge     | Constant    | 1       | 4,185  |
|            | 1C UDDS            | Drive Cycle | 0.5     | 6,000  |
| Testing    | 1.5C Discharge     | Constant    | 1       | 7,218  |
|            | 3.5C Discharge     | Constant    | 1       | 2,913  |
|            | 4.5C Discharge     | Constant    | 1       | 2,180  |
|            | 1C US06            | Drive Cycle | 0.5     | 6,000  |
|            | 1C DST             | Drive Cycle | 0.5     | 6,000  |
|            | 1C Pulse (1/60 Hz) | Square Wave | 0.5     | 6,000  |

concentration states  $c_{se,p}$  and  $c_{se,n}$ . Similarly, the bulk SOC is associated with the battery volume-averaged/steady-state behavior, e.g., open-circuit voltage, contained in the bulk concentration states  $\bar{c}_{s,p}$  and  $\bar{c}_{s,n}$ . Lastly, the anode electrolyte concentration  $c_{e,n}$  was selected to capture the dynamic behavior of the electrolyte gradient, which is sufficiently represented by the concentration in a single electrode (we chose the anode) due to symmetry. Thus, the complete input vector for the GPR model, as would be applied in Eqn. (7), is  $\mathbf{x}_k = \begin{bmatrix} I_k \\ s_k \end{bmatrix} = [I_k, SOC_{surf,k}, SOC_{bulk,k}, c_{e,n,k}]^T$ .

To collect data for training, validating, and testing the hybrid model, we experimentally measured the voltage response of a Kokam SLPB75106100 lithium-nickelmanganese-cobalt (NMC) pouch cell under a series of 14 input current profiles, using an Arbin LBT21084 cycler with a sub-microvolt measurement resolution. The input profiles were selected to span a wide array of operating conditions through different current amplitudes, SOC ranges, dynamics (e.g., constant current vs. dynamic drive cycle), and durations, as summarized in Table I. Table I also indicates the profile assignments for training, validation, and testing. All experiments were conducted at 25 °C with a measurement sampling interval of 0.3 seconds. The SPMe was configured with the parameter set identified in [25] for the same Kokam cell, yet with OCP-related parameters that were estimated under C/50 discharge data. We note that the performance of the SPMe in Section V is generally poor due to errors in this parameterization, which would not be acceptable in a realworld application (i.e., when the accuracy of the parameters is critical for model-based control and estimation). However, this configuration is appropriate for validating the hybrid model because it requires large residuals to be predicted under high parameter uncertainty—a challenging scenario.

The GPR input training matrix  $\boldsymbol{X}$  was generated by applying the SPMe to predict the internal state trajectories under each training profile, while the output residual training vector  $\boldsymbol{y}$  was computed by subtracting the SPMe voltage predictions from the measured voltage data. The training

TABLE II
PREDICTION RESULTS

| Group      | Input Profile      | SPMe RMSE $(mV)$ | Hybrid Model RMSE $(mV)$ | RER   |
|------------|--------------------|------------------|--------------------------|-------|
| Training   | 1C Discharge       | 161.7            | 3.8                      | 97.7% |
|            | 2C Discharge       | 197.9            | 2.8                      | 98.6% |
|            | 3C Discharge       | 211.8            | 1.1                      | 99.5% |
|            | 4C Discharge       | 235.8            | 3.1                      | 98.7% |
|            | 5C Discharge       | 276.9            | 1.8                      | 99.3% |
|            | 1C FUDS            | 7.4              | 1.5                      | 79.6% |
| Validation | 2.5C Discharge     | 215.7            | 16.6                     | 92.3% |
|            | 1C UDDS            | 8.0              | 2.2                      | 72.0% |
| Testing    | 1.5C Discharge     | 194.3            | 13.4                     | 93.1% |
|            | 3.5C Discharge     | 227.5            | 8.8                      | 96.1% |
|            | 4.5C Discharge     | 264.8            | 17.4                     | 93.4% |
|            | 1C US06            | 6.5              | 1.1                      | 83.4% |
|            | 1C DST             | 7.5              | 1.2                      | 83.7% |
|            | 1C Pulse (1/60 Hz) | 13.0             | 2.0                      | 84.6% |

covariance matrix K was then constructed with the squared exponential covariance function in Eqn. (7). Table I reveals that the six-profile training set comprises over 30,000 data points, yielding a  $30,377 \times 30,377$  element covariance matrix K that is intractable to invert. Since GPR is capable of performing well under sparse training data [9], we propose to sample an evenly distributed set of data points across the full span of each training profile for use in the model. In this work, we have selected a sample of 50 points per profile, yielding a lightweight  $300 \times 300$  covariance matrix that is computationally feasible.

Finally, the hyperparameters of the covariance function were computed by maximizing the log marginal likelihood of the prediction across the two validation profiles, according to Eqn. (11). Performing this optimization over the validation profiles instead of the training profiles has the two-fold benefit of increasing the diversity of the data that the model experiences and reducing the solution time due to the smaller number of data points. As with the training profiles, we sampled an evenly distributed set of 50 points across the full span of each validation profile, yielding a  $100 \times 100$  covariance matrix for the optimization.

## V. EXPERIMENTAL RESULTS

The hybrid model was implemented to predict the output voltage trajectory under each input profile and the results are presented in Table II. Prediction accuracy is quantified by the root-mean-square error (RMSE) between the predicted and measured output voltage trajectories, and results are provided for the standalone SPMe and hybrid model. In addition, the relative error reduction (RER) is listed, which describes the extent to which the SPMe prediction error is reduced by implementing the hybrid model [18],

$$RER = \frac{RMSE_{SPMe} - RMSE_{HM}}{RMSE_{SPMe}} \times 100\%.$$
 (12)

The hybrid model consistently achieved excellent prediction accuracy under the training profiles (RMSE  $\leq$  3.8 mV),

as expected. However, it is notable that the model was only trained with 50 points per profile (i.e., 0.45-2.6% of the total points, depending on the profile) and was able to yield accurate predictions for the remaining points. This attests to the predictive capability of GPR under sparse training data, and the effectiveness of downsampling for reducing the number of training data points without compromising prediction accuracy.

Upon applying the testing profiles, the hybrid model maintained high prediction accuracy with a maximum RMSE of 17.4~mV and mean RMSE of 7.3~mV. The RER was also consistently high (RER  $\geq 83.4\%$ ), indicating significant improvement in prediction accuracy over the standalone SPMe. The prediction errors were generally lower with higher RERs than those of the state-of-the-art neural-network-based electrochemical residual models in [16], [18], though a direct comparison is not possible due to the variations in the model, battery chemistry, and testing profiles. In addition, the hybrid model yielded comparable errors under the validation profiles (which were used to tune the hyperparameters), indicating that the model was not overfitted.

The testing predictions under 4.5C Discharge and 1C US06 are visualized in Figs. 2 & 3, respectively. These plots indicate the voltage measurements (solid black line), SPMe predictions (dotted red line), and hybrid model predictions (dashed green line) with the predicted 95% confidence interval (shaded green region). Each plot also features inset axes with a zoomed view of a highlighted region. Qualitatively, these plots illustrate the high prediction accuracy of the hybrid model outputs, which closely track the measurements with considerable improvement over the SPMe predictions. Most notably, Fig. 3 highlights the accuracy of the predicted 95% confidence interval, which generally encompasses the measurements and thus correctly captures the uncertainty due to random noise. However, this is not the case in Fig. 2, where the hybrid model prediction bias is large enough that the measurements are consistently outside of the confidence interval. Still, the confidence interval is appropriately sized as to encompass the noisy measurements if the predictions were unbiased. This relatively large prediction bias was attributed to the substantial prediction bias of the SPMe for this case. Finally, both plots illustrate the intrinsic filtering effect of GPR, in which the predictions are markedly smoother than the noisy measurements—a desirable effect for feedback control and estimation applications.

It is notable that the hybrid model yielded an accurate prediction of the 1C Pulse voltage response (RMSE =  $2.0\,mV$ ), although the model was neither trained nor validated (hyperparameters tuned) with a square-wave input profile. Thus, the predictions under 1C Pulse were based on constant-current and drive-cycle training data, which attests to the generalizability of the model under different types of input profiles.

Finally, the computational expense of the hybrid model was evaluated. The hyperparameter tuning procedure, detailed in Section IV, took 31 seconds on a laptop PC with an Intel i7-4720HQ 2.6 GHz quad-core processor. This

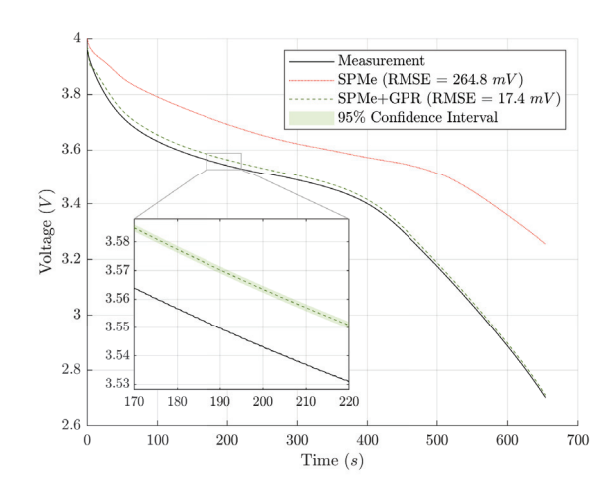


Fig. 2. Voltage predictions under 4.5C Discharge input profile.

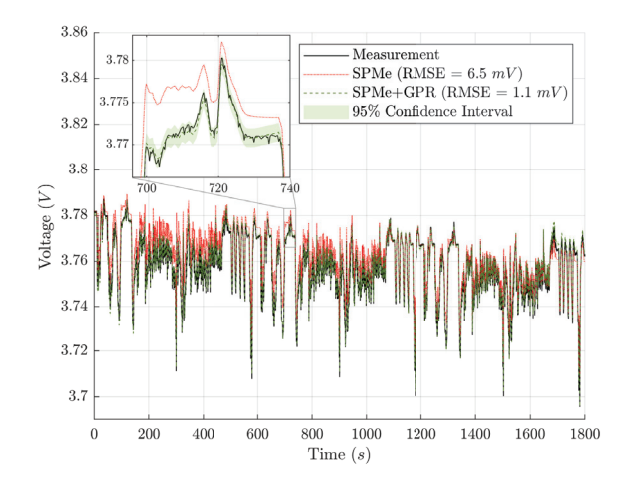


Fig. 3. Voltage predictions under 1C US06 input profile.

process is akin to the training procedure for parametric ML models, such as neural networks, as it only needs to be done once before the prediction phase, yet it can be much more efficient due to the smaller number of parameters (e.g., the feedforward neural networks developed in [18] each have over 1,248 trainable parameters while our proposed GPR model has 6). During the prediction phase, the computation time scales linearly with the number of time steps in the profile as the SPMe and GPR are iteratively executed. The mean computation time per time step across all 14 of the studied input profiles was 0.86 ms, which was split 25/75% between the SPMe/GPR models, respectively. Thus, for the 0.3-second time step used in this work, the ratio of computation time to modeled time is only 0.003, indicating excellent suitability for online applications. Therefore, through the high prediction performance and low computational expense, the proposed GPR-based hybrid modeling framework was validated as an efficient means for improving output prediction accuracy.

#### VI. CONCLUSIONS

In this work, we proposed a lightweight GPR-based hybrid modeling framework for efficiently improving the output prediction accuracy of electrochemical Li-ion battery models. The framework employs a data sampling procedure that utilizes a small distributed subset of the training and validation data for tuning the hyperparameters and computing predictions. By using training and validation data downsampled to less than 1%, the model was observed to generate predictions at an ample rate for online applications, through a measured ratio of computation time to modeled time of 0.003. Despite the sparsity of the training data, the accuracy of the model was experimentally validated through prediction RMSEs that were less than 18 mV, with a mean RMSE of 7.3 mV across all six testing profiles. Relative error reductions were greater than 83% for the testing profiles, indicating substantial improvements in output prediction accuracy over the standalone SPMe.

These results attest to the potential for GPR-based hybrid models to change the paradigm of battery modeling, especially in light of the emerging demands of advanced BMSs. Specifically, the exhibited capability for GPR to perform well under sparse training data indicates that the computational expense often associated with ML techniques can be mitigated through data sampling. We envision that representing the model/measurement uncertainty (i.e., voltage residual) as a Gaussian process can also facilitate the estimation of the parameters of the physics-based (electrochemical) model through an integrated hybrid model parameterization methodology, which is critical for accurate health monitoring and model-based control and estimation. We anticipate investigating this topic in future work.

## ACKNOWLEDGMENT

We appreciate the funding support from the NSF CA-REER Program (Grant No. 2046292) and the NASA HOME Space Technology Research Institute (Grant No. 80NSSC19K1052).

## REFERENCES

- [1] A. Allam and S. Onori, "On-line Capacity Estimation for Lithium-ion Battery Cells via an Electrochemical Model-based Adaptive Interconnected Observer," *IEEE Transactions on Control Systems Technology*, vol. 29, no. 4, pp. 1636–1651, Jul. 2021.
- [2] X. Lin, H. E. Perez, J. B. Siegel, A. G. Stefanopoulou, Y. Li, R. D. Anderson, Y. Ding, and M. P. Castanier, "Online parameterization of lumped thermal dynamics in cylindrical lithium ion batteries for core temperature estimation and health monitoring," *IEEE Transactions on Control Systems Technology*, vol. 21, no. 5, pp. 1745–1755, 2012.
- [3] L. D. Couto, R. Romagnoli, S. Park, D. Zhang, S. J. Moura, M. Kinnaert, and E. Garone, "Faster and Healthier Charging of Lithium-Ion Batteries via Constrained Feedback Control," *IEEE Transactions on Control Systems Technology*, vol. 30, no. 5, pp. 1990–2001, Sep. 2022.
- [4] C.-H. Chung, S. Jangra, Q. Lai, and X. Lin, "Optimization of electric vehicle charging for battery maintenance and degradation management," *IEEE Transactions on Transportation Electrification*, vol. 6, no. 3, pp. 958–969, 2020.
- [5] X. Pang, X. Liu, J. Jia, J. Wen, Y. Shi, J. Zeng, and Z. Zhao, "A lithium-ion battery remaining useful life prediction method based on the incremental capacity analysis and Gaussian process regression," *Microelectronics Reliability*, vol. 127, p. 114405, Dec. 2021.

- [6] N. A. Chaturvedi, R. Klein, J. Christensen, J. Ahmed, and A. Kojic, "Algorithms for Advanced Battery-Management Systems," *IEEE Control Systems*, vol. 30, no. 3, pp. 49–68, Jun. 2010.
- [7] L. Xu, F. Wu, R. Chen, and L. Li, "Data-driven-aided strategies in battery lifecycle management: Prediction, monitoring, and optimization," *Energy Storage Materials*, vol. 59, p. 102785, May 2023.
- [8] M. Aykol, C. B. Gopal, A. Anapolsky, P. K. Herring, B. Van Vlijmen, M. D. Berliner, M. Z. Bazant, R. D. Braatz, W. C. Chueh, and B. D. Storey, "Perspective—Combining Physics and Machine Learning to Predict Battery Lifetime," *Journal of The Electrochemical Society*, vol. 168, no. 3, p. 030525, Mar. 2021.
- [9] J. Willard, X. Jia, S. Xu, M. Steinbach, and V. Kumar, "Integrating Scientific Knowledge with Machine Learning for Engineering and Environmental Systems," ACM Computing Surveys, vol. 55, no. 4, pp. 1–37, Apr. 2023.
- [10] M. Doyle, T. F. Fuller, and J. Newman, "Modeling of Galvanostatic Charge and Discharge of the Lithium/Polymer/Insertion Cell," *Journal* of The Electrochemical Society, vol. 140, no. 6, pp. 1526–1533, Jun. 1993.
- [11] G. Ning and B. N. Popov, "Cycle Life Modeling of Lithium-Ion Batteries," *Journal of The Electrochemical Society*, vol. 151, no. 10, p. A1584, 2004.
- [12] X. Lin, Y. Kim, S. Mohan, J. B. Siegel, and A. G. Stefanopoulou, "Modeling and estimation for advanced battery management," *Annual Review of Control, Robotics, and Autonomous Systems*, vol. 2, pp. 393–426, 2019.
- [13] J. Fogelquist, Q. Lai, and X. Lin, "On the Error of Li-ion Battery Parameter Estimation Subject to System Uncertainties," *Journal of The Electrochemical Society*, vol. 170, no. 3, p. 030510, Mar. 2023.
- [14] X. Hu, Y. Che, X. Lin, and S. Onori, "Battery Health Prediction Using Fusion-Based Feature Selection and Machine Learning," *IEEE Transactions on Transportation Electrification*, vol. 7, no. 2, pp. 382–398, Jun. 2021.
- [15] G. Pozzato and S. Onori, "Combining Physics-Based and Machine Learning Methods to Accelerate Innovation in Sustainable Transportation and Beyond: A Control Perspective," in 2023 American Control Conference (ACC). San Diego, CA, USA: IEEE, 2023, pp. 640–653.
- [16] S. Park, D. Zhang, and S. Moura, "Hybrid Electrochemical Modeling with Recurrent Neural Networks for Li-ion Batteries," in 2017 American Control Conference (ACC). Seattle, WA, USA: IEEE, May 2017, pp. 3777–3782.
- [17] Z. Xi, M. Dahmardeh, B. Xia, Y. Fu, and C. Mi, "Learning of Battery Model Bias for Effective State of Charge Estimation of Lithium-Ion Batteries," *IEEE Transactions on Vehicular Technology*, vol. 68, no. 9, pp. 8613–8628, Sep. 2019.
- [18] H. Tu, S. Moura, Y. Wang, and H. Fang, "Integrating physics-based modeling with machine learning for lithium-ion batteries," *Applied Energy*, vol. 329, p. 120289, Jan. 2023.
- [19] C. E. Rasmussen and C. K. I. Williams, Gaussian processes for machine learning, ser. Adaptive computation and machine learning. Cambridge, Mass: MIT Press, 2006.
- [20] R. Tuo and C. F. J. Wu, "A theoretical framework for calibration in computer models: parametrization, estimation and convergence properties," SIAM/ASA Journal on Uncertainty Quantification, vol. 4, no. 1, pp. 767–795, 2016.
- [21] S. J. Moura, F. B. Argomedo, R. Klein, A. Mirtabatabaei, and M. Krstic, "Battery State Estimation for a Single Particle Model With Electrolyte Dynamics," *IEEE Transactions on Control Systems Technology*, vol. 25, no. 2, pp. 453–468, Mar. 2017.
- [22] Q. Lai, S. Jangra, H. J. Ahn, G. Kim, W. T. Joe, and X. Lin, "Analytical derivation and analysis of parameter sensitivity for battery electrochemical dynamics," *Journal of Power Sources*, vol. 472, pp. 228–338, 2020.
- [23] G. O. Sahinoglu, M. Pajovic, Z. Sahinoglu, Y. Wang, P. V. Orlik, and T. Wada, "Battery State-of-Charge Estimation Based on Regular/Recurrent Gaussian Process Regression," *IEEE Transactions on Industrial Electronics*, vol. 65, no. 5, pp. 4311–4321, May 2018.
- [24] R. R. Richardson, C. R. Birkl, M. A. Osborne, and D. A. Howey, "Gaussian Process Regression for In Situ Capacity Estimation of Lithium-Ion Batteries," *IEEE Transactions on Industrial Informatics*, vol. 15, no. 1, pp. 127–138, Jan. 2019.
- [25] W. Li, I. Demir, D. Cao, D. Jöst, F. Ringbeck, M. Junker, and D. U. Sauer, "Data-driven systematic parameter identification of an electro-chemical model for lithium-ion batteries with artificial intelligence," *Energy Storage Materials*, vol. 44, pp. 557–570, Jan. 2022.